

Efficient Direct Recycling of Degraded LiMn_2O_4 Cathodes by One-Step Hydrothermal Relithiation

Hongpeng Gao, Qizhang Yan, Panpan Xu, Haodong Liu, Mingqian Li, Ping Liu, Jian Luo, and Zheng Chen*



Cite This: *ACS Appl. Mater. Interfaces* 2020, 12, 51546–51554



Read Online

ACCESS |



Metrics & More



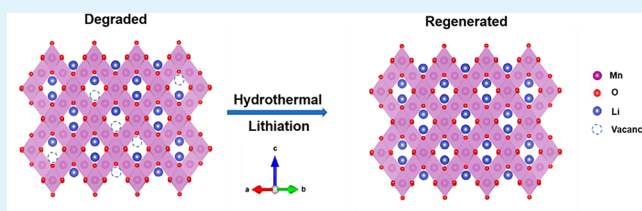
Article Recommendations



Supporting Information

ABSTRACT: Due to the large demand of lithium-ion batteries (LIBs) for energy storage in daily life and the limited lifetime of commercial LIB cells, exploring green and sustainable recycling methods becomes an urgent need to mitigate the environmental and economic issues associated with waste LIBs. In this work, we demonstrate an efficient direct recycling method to regenerate degraded lithium manganese oxide (LMO) cathodes to restore their high capacity, long cycling stability, and high rate performance, on par with pristine LMO materials. This one-step regeneration, achieved by a hydrothermal reaction in dilution Li-containing solution, enables the reconstruction of desired stoichiometry and microphase purity, which is further validated by testing spent LIBs with different states of health. Life-cycle analysis suggested the great environmental and economic benefits enabled by this direct regeneration method compared with today's pyro- and hydrometallurgical processes. This work not only represents a fundamental understanding of the relithiation mechanism of spent cathodes but also provides a potential solution for sustainable and closed-loop recycling and remanufacturing of energy materials.

KEYWORDS: lithium-ion batteries, recycling, direct regeneration, lithium manganese oxide, life-cycle analysis, sustainability



INTRODUCTION

Among the state-of-art energy storage technologies, lithium-ion batteries (LIBs) have dominating applications in portable electronics, electric vehicles (EVs), and stationary energy storage.^{1,2} The LIB industry has experienced a revolutionary development in the past decade with remarkable performance improvements, satisfying many key performance requirements such as high energy density, high power density, and good cycling stability.³ The global market of LIB expands dramatically as a result of the significant growth in the xEV market recent years, representing more than 180 GWh of worldwide LIB sales in 2018. Considering the limited service life for EVs applications (about 8–10 years) and the environmental impact of inappropriate battery disposal, there is an urgent need to develop efficient and sustainable methods for recycling/regenerating the materials out of spent LIBs.^{4,5}

The state-of-the-art approaches in the LIB recycling industry are mainly based on hydrometallurgical and pyrometallurgical processes.^{6,7} Both methods involve energy-intensive or caustic processes such as sintering, acid leaching, and chemical precipitation, which are unavoidably associated with heavy CO_2 emission and other waste generation.^{8,9} These methods can be viable in processing Co-containing LIBs since the value of Co products (e.g., CoSO_4) may compensate for the high operation cost. However, for many other LIBs, such as LiMn_2O_4 (LMO) batteries, the low intrinsic value of their elemental components (e.g., Mn) poses huge challenges for

recycling via traditional ways.¹⁰ Nevertheless, such low-cost batteries offer unique properties for many applications. For example, LMO is an appealing cathode material due to its high thermal stability and low cost. These features make it attractive for low-cost EVs and large-scale energy storage.

On the other hand, direct regeneration without a destructive high-temperature smelting and acid-leaching process is attracting considerable attention, as it can potentially provide a cost-reduction and environmentally benign solution for recycling useful materials from spent batteries. Various methodologies have been demonstrated for direct regeneration of layered oxide cathode, such as LiCoO_2 (LCO) and $\text{LiNi}_x\text{Co}_y\text{Mn}_z\text{O}_2$ (or NCM, $x + y + z = 1$). These include electrochemical treatment,¹¹ hydrothermal relithiation,¹² ionothermal lithiation,¹³ molten salt relithiation,¹⁴ and solid-state sintering¹⁵ approaches. For example, Shi et al. have recently demonstrated a direct regeneration method of NCM, with the first discharge capacity of 158 mAh/g and the retention of 77.8% after 100 cycles at 1 C via combining hydrothermal treatment and short-annealing process.¹⁶ Wang et al.

Received: September 1, 2020

Accepted: October 20, 2020

Published: November 5, 2020



successfully regenerated spent NCM via a cost-effective Li halide as the Li source in ionic liquids with the advantages of low vapor pressures.¹³ Li et al. provide a promising improvement on treating the spent NCM by a water process that avoids the usage of *N*-methyl-2-pyrrolidone (NMP).¹⁷ In spite of the successful demonstration of the direct regeneration of LIBs containing high-value transition elements (e.g., Co, Ni), only a few studies have been done on regenerating cathodes with low cost such as LMO.^{18,19} The direct recycling by extraction of valuable elements via supercritical carbon dioxide (CO₂) has been demonstrated to be costly and not worthy in the case of LMO batteries.²⁰

By leveraging the knowledge established in developing various synthesis methods for spinel cathode materials,^{21–23} in this work, we demonstrated an one-step direct regeneration method to effectively recycle spent LMO cathodes, which showed successful reconstruction of the stoichiometric composition and restored crystallinity from severely degraded LMO cathode materials with different states of health (SOH). Specifically, we used a hydrothermal treatment with dilute lithium hydroxide (LiOH) solution to simultaneously relithiate degraded LMO particles and heal the microstructure defects. Figure 1 illustrates the relithiation process highlighting the

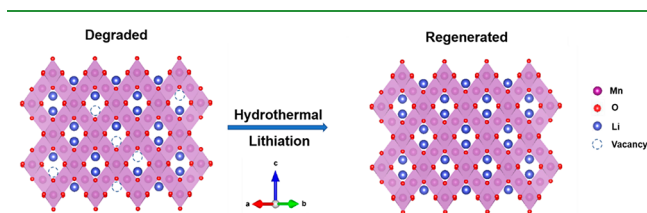


Figure 1. Illustration of the hydrothermal lithiation process in which Li⁺ is redosed to the Li-deficient sites to recover its desired stoichiometry.

migration of lithiation inside the spinel structure along the (110) direction during the hydrothermal process. The reasons for capacity fading have been investigated in the past decade, which are mainly ascribed to Li loss,²⁴ Mn migration,²⁵ and John–Tell distortion.^{26,27} By tuning the operation conditions, the composition and structure evolution of LMO during the regeneration process was systematically investigated via various physicochemical characterizations. The study on the kinetic mechanism combined with neutron diffraction indicates that the lithium loss and lattice distortion can be fully recovered to the original levels of the pristine materials. This work provides a new direction toward cost-effective and environmentally friendly battery recycling to potentially address the sustainability issues related to LIBs.

EXPERIMENTAL SECTION

Commercial Level Pouch Cell Assembly. Dry pouch cells (500 mAh) made with lithium manganese oxide (LMO) as cathode active materials and graphite as anode active materials were directly supplied from Guangdong Canrd New Energy Technology Co., Ltd., China. The electrolyte was battery grade lithium hexafluorophosphate (LiPF₆) solution in ethylene carbonate (EC) and dimethyl carbonate (DEC) purchased from Sigma-Aldrich, with the composition of 1.0 M LiPF₆ in EC/DEC = 50/50 (v/v) (LP40). The dry pouch cells were filled by 1 mL of electrolyte and sealed by the vacuum sealer machine (MTI Corp.) inside the glovebox. After 24 h standing time, the pouch cells were activated in the voltage window of 3–4.3 V by C/10 (50 mA) (1 C = 148 mA/g) under constant current–constant voltage

(CC–CV) cycling with the cutoff current at C/20 (25 mA). The activated pouch cells were cycled between 3.0 and 4.3 V at 1.5 C (750 mA) for 40 cycles and then 0.5 C (250 mA) for the other 160 cycles.

Homemade Single-Layer Pouch Cell Assembly. Single-layer LMO–graphite pouch cells were also built in our lab to investigate the lithium distribution in the cycled cells. The pristine LMO powders (MTI Corp.) were mixed with poly(vinylidene fluoride) (PVDF, KYNAR 2800) and carbon black (Super P65) in NMP (Sigma-Aldrich, anhydrous, 99.5%) at a mass ratio of 8:1:1 to form homogeneous slurries. The slurries were cast by a doctor blade and then dried under vacuum at room temperature for 2 h followed by drying at 80 °C for 6 h. After rolling, the cathodes were cut into 4.4 cm × 5.7 cm with a mass loading of 6.8 mg/cm². The prebaked graphite (Graphite & Carbon Products, G80) was mixed with PVDF and Super P65 in NMP at a mass ratio of 90:5:5. The slurries were cast by a doctor blade and then dried under vacuum at 80 °C for 6 h. After rolling, the anodes were then cut into 4.5 cm × 5.8 cm with a mass loading of 3.7 mg/cm². After the electrodes were matched under a controlled N/P ratio (1.1–1.15), single-layer pouch cells were assembled with a trilayer membrane (Celgard 2320) as the separator and 500 μL of LP40 as the electrolyte. All the homemade pouch cells were activated in the voltage window of 3–4.3 V at C/10 under CC–CV cycling with the cutoff current of C/20. The cells were cycled between 3.0 and 4.3 V at C/2 under CC–CV with the cutoff current C/5 for 200 cycles.

Cathode Materials Harvesting. All the pouch cells were discharged to 2.8 V before disassembly. The cathode strips were harvested from both the commercial and homemade pouch cells, by thoroughly rinsing with dimethyl carbonate (DMC), and then soaked in NMP for 6 h under 50 °C. The active materials, binder, and carbon black were removed from the aluminum substrates by sonification and scrapping. After the NMP suspension was centrifuged at 3500 rpm for 5 min, active materials were precipitated. The precipitation was washed several times by NMP. Then the active materials were collected and dried under vacuum at 80 °C overnight for regeneration.

Regeneration of Cathode Materials. For the hydrothermal treatment, 0.25 g of cycled LMO materials was added into a 100 mL Teflon-lined autoclave filled with 80 mL of lithium hydroxide (LiOH) solution with different concentrations. The autoclaves were consistently heated at 180 °C for different periods of time. After cooling down naturally to room temperature, the treated powders were washed by deionized water at least 5 times until pH ~ 7 and then dried under vacuum at 80 °C overnight.

Characterization of Regenerated Materials. The compositions of cycled/regenerated LMO cathode materials were measured by an inductively coupled plasma quadrupole mass spectrometer (ICP-MS, Thermo Scientific, iCAP RQ model). Their crystal structures were examined by X-ray powder diffraction (XRD) employing a Bruker D2 Phaser (Cu Kα radiation, λ = 1.5406 Å) from a scanning rate of 0.58 deg/min.

Time-of-flight (TOF) powder neutron diffraction was measured at the VULCAN instrument at the Spallation Neutron Sources (SNS), Oak Ridge National Laboratory (ORNL).²⁸ The diffraction pattern was measured at the detector banks at 2θ = ±90°, equipped with 5 mm receiving collimators. Neutron powder diffraction patterns were collected in the high-intensity mode (Δd/d ~ 0.45%) for a duration of 2 h under the nominal 1.4 MW SNS operation and then processed using VDRIVE software.²⁹ Rietveld refinement against the neutron diffraction was performed using General Structure Analysis System (GSAS) software with an EXPGUI interface.^{30,31}

The morphology of the pristine, cycled, and regenerated LMO powder was observed by Scanning Electron Microscope (SEM, FEI XL30). The particle size distribution was analyzed with the Nano Measurer software. The microstructures of the regenerated LMO powder were further confirmed by high-resolution transmission electron microscopic (HR-TEM) images which were collected on a JEOL-2800 at 200 kV with a Gatan OneView Camera (25 fps, full 4 K resolution). The detailed structure information was measured by DigitalMicrograph (DM). X-ray photoelectron spectroscopic (XPS)

measurement was conducted with an AXIS Supra by Kratos Analytical with an Al K α anode source working at 15 kV and 10⁻⁸ Torr chamber pressure. The spectra data were processed by CasaXPS software. All spectra were calibrated with the hydrocarbon C 1s peak at 284.6 eV. The XPS depth profile analysis was carried out with a gas cluster ion source (GCIS) using a focused energetic Ar ion beam.

Analysis of Lithium Distribution in Cycled Pouch Cells. After cycling at 0.5 C under CC–CV with a cutoff current of 0.1 C for 200 cycles, the homemade pouch cells were disassembled in a glovebox. Ten microliters of electrolyte was collected by a pipet and diluted into 10 mL of DMC. The anodes were rinsed by DMC for 2 h and then soaked in 1 M HCl for 3 days. The cathode active materials were collected by the same method as harvesting commercial pouch cells described above. The compositions of electrolyte, anode electrodes, and cathode electrodes were measured by ICP-MS.

Electrochemical Characterization. The active materials were mixed with PVDF and Super P65 in NMP at a mass ratio of 8:1:1. Then the formed slurries were cast on an aluminum foil using a doctor blade and dried in vacuum at 80 °C for 6 h. The LMO cathodes were cut and compressed by rolling. The areal mass loadings of LMO electrodes for coil cells were around 10 mg/cm². Coin cells were assembled with a Li metal disc (thickness 1.1 mm) as the counter electrode, LP40 as the electrolyte, and a trilayer membrane (Celgard 2320) as the separator. Galvanostatic charge–discharge was carried out using a Neware battery testing system in the potential range of 3.0–4.3 V at 0.5 C for 200 cycles after C/10 in the initial cycle and 0.3 C in the following two cycles.

RESULTS AND DISCUSSION

Both commercial and homemade pouch cells were used for the demonstration of our direct recycling approach. The details for assembling different pouch cells are described in the experimental section (Supporting Information). All the pouch cells were cycled in the voltage window of 3.0–4.3 V until more than 20% capacity degradation was obtained (Figure S1). The LMO cathode materials were collected and purified by a typical procedure developed in our previous work.¹⁵ The obtained cathode particles with composition and structure degradation were subject to the hydrothermal treatment (denoted as “HT”) under different conditions. The regenerated cathode particles were carefully characterized and made into new cells to evaluate the electrochemical performance. We first analyzed the cell components to identify the sources of capacity degradation associated with composition changes. For more quantitative analysis, homemade LMO/graphite single-layer pouch cells with controlled cathode mass were used to investigate the Li distribution in degraded cells under room temperature. After 200 cycles in a voltage range of 3.0–4.3 V at 0.5 C, 20% capacity fading appeared in our homemade pouch cells (Figure S2). The causes of capacity loss of the full cell are complicated, including the SEI formation on the anode surface, lattice distortion caused by the John–Tell effect,²⁷ and Mn(II) dissolution induced by Mn(III) disproportionation.^{32,33} To identify the Li distribution, the graphite and LMO electrodes from a cycled LMO pouch cell were immersed in diethyl carbonate (DEC) solution separately to wash out the residual electrolyte. Then the anode and cathode active materials were scratched off their current collectors and soaked into hydrochloric acid to extract metal elements. A complete analysis was conducted to investigate the distribution of Li coming from the cathode side. Figure S3 shows that 82.6% of Li was retained inside the degraded spinel cathode particles and 13.5% of Li in anode where the consumption of Li was likely associated with the formation of thick SEI during long-term cycling.³⁴ Interest-

ingly, 0.8 mM Mn was detected in 1 M LiPF₆ EC/DEC electrolyte. In William’s work, the same level of Mn concentration was detected after the LMO powders were exposed to the electrolyte. Although the appreciable Mn dissolution may cause the structure degradation, the overall loss of Li dominates the capacity fading compared with the small amount of Mn loss in the cathodes.³⁵ Thus, the compensation of the Li loss is a critical step to fix the degradation issues of the LMO cathode for regeneration. The compositions of cycled and regenerated LMO cathode materials were measured by an inductively coupled plasma quadrupole mass spectrometer (ICP-MS) (Table 1). Note that

Table 1. Lattice Parameters and ICP Results of the Pristine, Cycled, and Regenerated LMO Particles^a

sample	<i>a</i> /Å	<i>R</i> _{wp} /%	<i>R</i> _p /%	composition
pristine LMO	8.2275(2)	3.93	2.05	Li _{1.058} Mn _{1.951} O _{3.932}
cycled LMO	8.1930(4)	3.53	1.90	Li _{0.885} Mn _{1.943} O _{3.942}
0.02 M HT-LMO	8.2218(3)	3.51	3.00	Li _{1.033} Mn _{1.945} O _{3.939}
0.1 M HT-LMO	8.2272(2)	3.39	2.63	Li _{1.060} Mn _{1.942} O _{3.944}
0.2 M HT-LMO	8.2274(3)	2.76	1.65	Li _{1.067} Mn _{1.933} O _{3.944}

^aThe LMO sample regenerated in 0.02, 0.1, and 0.2 M of LiOH for 12 h was named as 0.02M HT-LMO, 0.1M HT-LMO, and 0.2M HT-LMO, respectively.

the imperfect stoichiometry from the composition of commercial LMO particles is often designed for the extension of the cycle life, and the oxygen defects are caused by their high-temperature sintering process.³⁶ The cycling data of commercial pouch cells (Figure S1) show that the capacity loss was more than 20% after 200 cycles under room temperature. The composition data in Table 1 show that the cathode material had 13% of Li loss compared with the pristine LMO even though the cells were discharged at a cutoff voltage at 3.0 V.

To design an optimal regeneration process, we first investigated the relithiation kinetics during the hydrothermal treatment process in 0.1 M LiOH at 180 °C (Figure 2a). Table S1 reveals that the Li composition can reach to the pristine level (e.g., 1.06 Li per Mn) after being treated for 6 h. Further extending the treatment time up to 12 h does not cause a continuous increase of the Li concentration in the solid LMO particles, which was confirmed by the refinement XRD (Figure 2b–d). In addition, cell-cycling performance (Figure S4) indicates that the 12 h treatment sample has been regenerated to the commercial reusable LMO cathode (to be discussed subsequently), which maintains high crystallinity and pure single phase.

Concentration of Li⁺ in the hydrothermal solution is also an important parameter determining the relithiation behavior. With the concentration of LiOH solution changed from 0.02 to 0.2 M, the degraded LMO particles can be fully recovered to reach the desired stoichiometry (~1.0 Li per Mn) at 180 °C for 12 h. As shown in Table 1, the composition of the regenerated LMO is sensitive to the concentration of the LiOH solution. When the LiOH concentration reached 0.4 M, more Li⁺ can be inserted into the lattice forming lithium-rich Li₂MnO₃ phase, as shown in Figure 3a with the increased intensity of impurity peaks at 18.8, 37.0, and 44.8 deg (marked by a star). These peaks are in a perfect match with (001), (130), and (131) peaks of the C2/*m* layered phase of Li₂MnO₃.^{37,38}

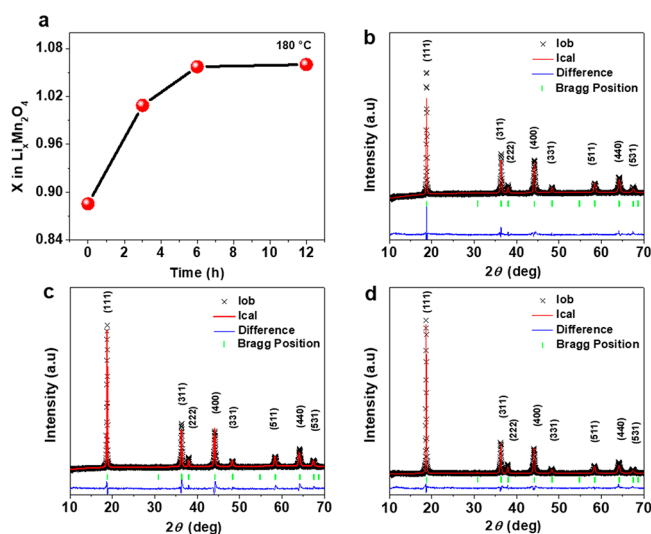


Figure 2. (a) Lithiation kinetics of degraded LIB cathode particles during hydrothermal treatment. The LMO sample regenerated in 0.1 M of LiOH was named as HT-3h-LMO, HT-6h-LMO, and HT-12h-LMO, respectively. Refinement XRD pattern of regenerated LMO particles: (b) HT-3h LMO, (c) HT-6h LMO, and (d) HT-12h LMO.

It is also critical to further investigate the evolution of the crystal structure of degraded LMO during the hydrothermal reaction. X-ray diffraction (XRD) patterns of cycled, pristine, and regenerated LMO are shown in Figure 3. The standard pattern of the spinel phase with the $Fd\bar{3}m$ space group was validated in all samples.³⁹ Although no additional impurity peaks exist, the peaks became broader and less intense in cycled LMO compared to pristine LMO. A shift of the major (111) spinel peaks to higher angles can also be clearly found in Figure 3b, corresponding to the lattice parameter shrinkage from 8.23 to 8.19 Å. It indicates that, although the spinel structure was retained, the more Li^+ removed from their tetrahedral sites, the more the decrease of unit-cell dimension are observed.⁴⁰ Thus, it is reasonable that the extent of Li^+ loss can be reflected on the right shift of (111) peaks which allows us to validate the effectiveness of our regeneration method. For example, after hydrothermal treatment in 0.1 M LiOH for 12 h, the (111) peak shifts back to lower angles and with intensity recovered to the pristine level. These results suggest the successful reconstruction of the crystal structure and high crystallinity of the regenerated LMO product.

Rietveld refinement was performed on all the XRD patterns using the General Structure Analysis System (GSAS) software

(Figure S5). Both R_B (Bragg factor) and R_{wp} (weighted profile R-factor) are less than 5% which indicates the reliability of the refinement results. The lattice parameters of all the samples are compared in Table 1. The results further validate that not only the Li loss is compensated but also the structure can be repaired after simple hydrothermal treatment. For the purpose of demonstration, hydrothermal relithiation with 0.1 M of LiOH at 180 °C for 12 h was selected to treat the degraded LMO cathode particles for the next step.

To further quantify the occupancy of Li sites inside the lattice, neutron diffraction measurement was conducted on the pristine, cycled, and regenerated LMO from 0.1 M of LiOH (Figure 4). As we expected, it evidently indicates that Li, Mn, and O are located on the 8a (tetrahedral), 16d (octahedral), and 32e Wyckoff sites, respectively.^{41,42} The Rietveld refinement results are listed in Table 2. The average Mn oxidation state increased from 3.52 to 3.60 during the long-term cycling because the Li vacancies appear inside the spinel lattice. After hydrothermal treatment, the average Mn oxidation state decreased back to 3.54, and the lattice parameter of the face-centered cubic (FCC) conventional unit cell increased from 8.1955(2) to 8.2280(3) Å due to the complement of Li into the vacancies. The decrease of the Mn–O bond length in cycled LMO is ascribed to the reduction of the Mn radius, whereas the radius of Mn^{4+} (0.530 Å) is smaller than that of Mn^{3+} ion (0.645 Å).⁴³ After regeneration, the bond length was resumed to the pristine value. In addition, the changes of the composition were also consistent with the structure parameters (Table 2), which further confirms that the degraded LMO cathode was successfully regenerated in 0.1 M LiOH solution.

The SEM images and size distribution of the pristine, cycled, and regenerated LMO particles are displayed in Figure S7. The pristine LMO sample has random particle morphology with peak sizes of about 1.2 μm . After long-term cycling, the peak size of LMO particles increased to 1–2 μm possibly due to aggregation. After hydrothermal treatment, the spent LMO particles become more uniform and maintain a narrow distribution similar to the pristine LMO sample. To obtain more insights in the microstructure, the regenerated cathode materials were carefully examined by high-resolution transmission electron microscope (HRTEM) (Figure 5a–b). The interplanar spacings of regenerated LMO were measured to be 0.48 and 0.25 nm, which corresponds to the orientation of the (111) and (311) atom plane found in typical LMO, respectively.^{44–46} The fast Fourier transform (FFT) patterns are indexed to the diffraction of the $\langle 011 \rangle$ and $\langle 010 \rangle$ zone axes.⁴⁷ Thus, the HRTEM images also confirm the

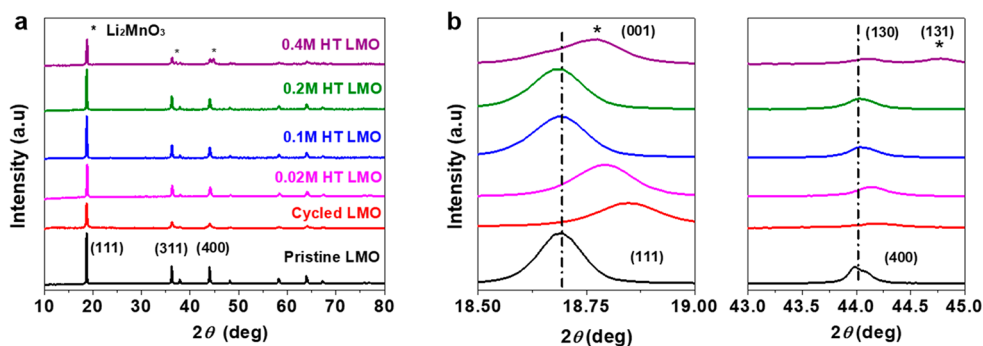


Figure 3. XRD patterns of pristine, cycled, and regenerated (a) LMO particles by hydrothermal treatment under 0.02, 0.1, 0.2, and 0.4 M LiOH solution; (b) enlargement of the regions in the range of 18.5–19.0° and 43–45°.

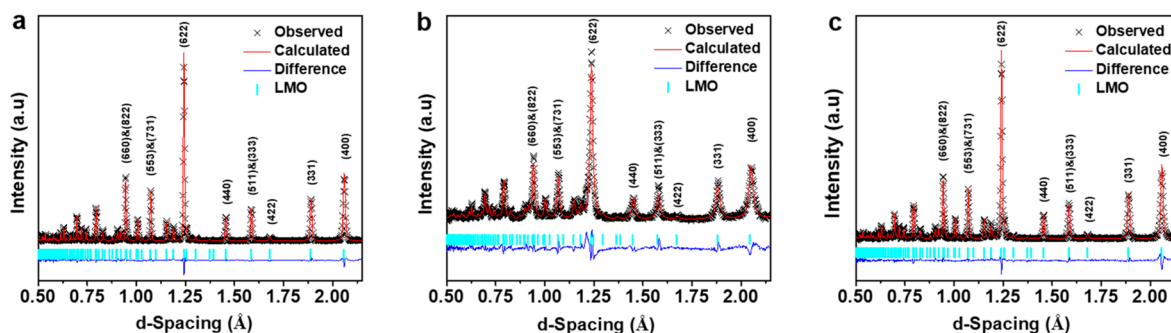


Figure 4. Rietveld refinement results of neutron diffraction patterns of (a) pristine, (b) cycled, and (c) regenerated LMO particles from 0.1 M of LiOH.

Table 2. Neutron Diffraction Refinement Results of Pristine, Cycled, and Regenerated LMO

sample	$a/\text{\AA}$	Mn–O bond length/ \AA	oxide state	composition
pristine LMO	8.2307(2)	1.954	+3.52	$\text{Li}_{1.058}\text{Mn}_{1.942}\text{O}_{3.944}$
cycled LMO	8.1955(2)	1.943	+3.60	$\text{Li}_{0.896}\text{Mn}_{1.942}\text{O}_{3.944}$
0.1 M HT-LMO	8.2280(3)	1.953	+3.54	$\text{Li}_{1.066}\text{Mn}_{1.934}\text{O}_{3.952}$

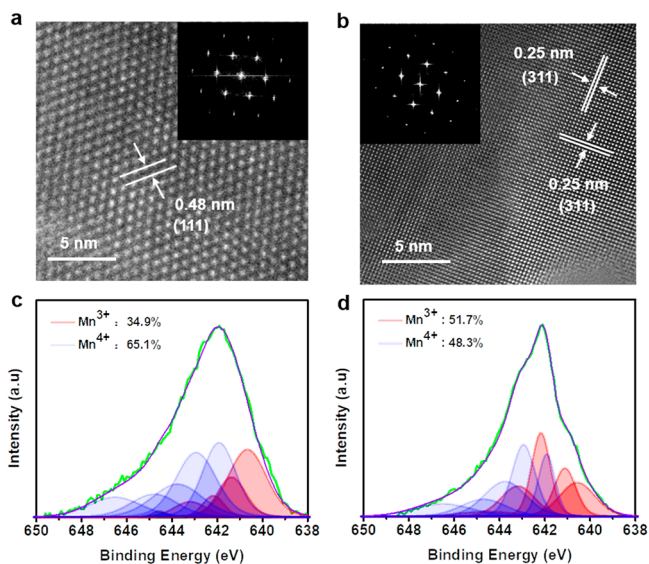


Figure 5. (a) HRTEM images and FFT patterns of regenerated LMO particles in the bulk region and (b) surface region. (c) XPS spectra of cycled LMO and (d) regenerated LMO particles.

reconstruction of the spinel structure in the regenerated LMO. Additional HRTEM images of cycled LMO particles in the surface and bulk regions are shown in Figure S8.

X-ray photoelectron spectroscopic (XPS) measurement was performed on cycled and regenerated LMO to investigate the changes of the valence status (Figure 5c–d). Peak fitting was conducted on the Mn $2p_{3/2}$ spectrum to provide a detailed distribution of the valence information on Mn in both samples (Tables S2 and S3).^{48,49} Figure 5c shows a broad shoulder in the region of high bonding energy, which can be ascribed to the high Mn^{4+} composition. Figure 5d shows a clear shoulder in the low bonding energy region indicating the Mn^{3+} contribution. Quantitative analysis reveals that 51.7% and 48.3% of Mn can be assigned to Mn^{3+} and Mn^{4+} , respectively,

in the regenerated cathode, which is in good agreement with the valence distribution of Mn in typical LMO. By comparison, 34.9% Mn^{3+} and 65.1% Mn^{4+} were found in cycled cathode. The increase of the average valence state of Mn can be attributed to the Li loss inside the lattice. Therefore, the more dominant contribution of Mn^{4+} in the cycled cathodes and its disappearance in regenerated cathodes further support that the Li-deficient spinel phases formed after cycling were recovered into well-defined, less defective structure after regeneration.

To evaluate the electrochemical performance of the pristine, cycled, and regenerated LMO samples, a galvanostatic charge/discharge test was conducted in a voltage range of 3.0–4.3 V. To compare the different electrochemical performance achieved with LMO regenerated in LiOH solution with different concentrations, differential capacity plots (dQ/dV) at the first cycle at 0.1 C were also acquired (Figure 6a). Unlike the broad peak of the 0.02 M regenerated sample, the LMO regenerated in 0.1 M of LiOH displayed sharp intrinsic reduction peaks at 4.16 and 4.03 V (labeled as R_1 and R_2) and oxidation peaks at 4.11 and 3.97 V (labeled as O_1 and O_2), which can be ascribed to the two-step mechanism of the electrochemical Li^+ intercalation and extraction from tetra-

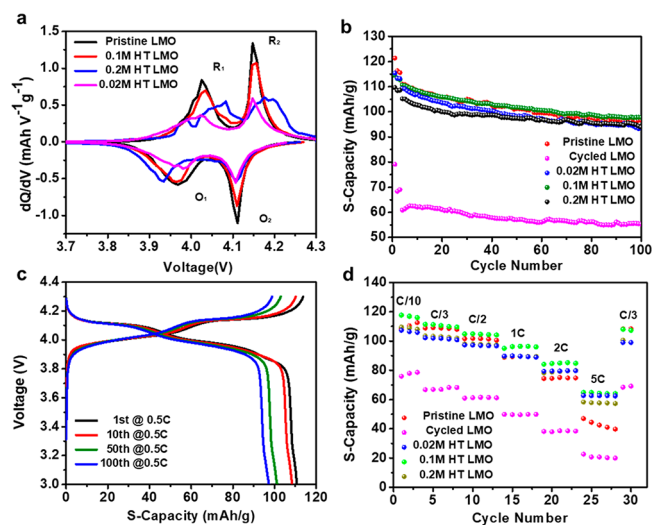


Figure 6. (a) dQ/dV plots of pristine and regenerated LMO samples at 0.1 C. (b) Cycling performance of pristine, nontreated, and regenerated LMO samples at 0.5 C. (c) Charge/discharge curve of LMO regenerated in 0.1 M of LiOH at the 1st, 10th, 50th, and 100th cycle at 0.5 C. (d) Rate performance of different LMO samples. HT-LMO: hydrothermal treatment at 180 °C for 12 h in LiOH solution with different concentrations.

dral sites in the spinel structure.^{50,51} The peak separations between charge and discharge scan are 57 and 61 mV, respectively, which is a good indication of the high reversibility of the electrochemical reaction, with small polarization and favorable reaction kinetics.⁵²

For LMO regenerated from 0.2 M of LiOH, two tiny split peaks were obtained instead of only one reduction peak (R_1), indicating the unexpected side reaction at the initial activation cycle. It also caused a relatively lower initial columbic efficiency (82%) compared with 90% of LMO obtained in 0.1 M LiOH. Furthermore, the larger peak separation suggests more severe polarization and poorer reversibility.

As shown in Figure 6b, the pristine LMO cathode showed a discharge capacity of 112 mAh/g at the first cycle at 0.5 C (1 C = 148 mAh/g) and 97 mAh/g after 100 cycles, corresponding to a capacity retention of 86.6%. The cycled LMO cathode (harvested from spent cells without any treatment) showed a discharge capacity of only 61 mAh/g at the first cycle at 0.5 C and 55 mAh/g after 100 cycles, which is expected again due to the Li^+ loss and irreversible lattice distortion. By hydrothermal treatment at 180 °C for 12 h, the electrochemical properties were fully recovered: a discharge capacity of 109, 111, and 105 mAh/g at the first cycle at 0.5 C and 94, 98, and 94 mAh/g after 100 cycles were obtained by LMO treated in 0.02, 0.1, and 0.2 M LiOH, respectively. In addition, the cycling stability of LMO was also recovered. For example, with the hydrothermal treatment in 0.1 M LiOH solution, the cycling stability of regenerated LMO was fully recovered to 88% capacity retention after 100 cycles, which was slightly improved even compared with the pristine LMO. Interestingly, both LMO samples obtained in 0.02 and 0.2 M LiOH showed slightly lower initial capacity compared with the sample regenerated in 0.1 M LiOH solution. That can be ascribed to the remaining Li deficiencies in 0.02 M HT LMO and phase impurity in 0.2 M HT LMO samples, which is consistent with the structure information described earlier.

In addition, compared with cycled LMO and LMO regenerated in 0.1 M of LiOH, the sharp peak indicates that the well-defined spinel structure with remarkable electrochemistry activity and high crystallinity was obtained by 0.1 M HT treatment. Two distinguished plateaus in the charge/discharge curves at the 1st, 10th, 50th, and 100th cycles are shown in Figure 6c, corresponding to two sharp peaks in differential capacity plots (Figure 6a), indicating the good cycling and crystalline stability.⁵³ The rate performance of the pristine, cycled, and regenerated LMO cathodes materials is shown in Figure 6d. The 0.1 M HT LMO showed an improved capacity at high rates compared with pristine LMO particles. For example, the 0.1 M HT LMO electrode delivered a specific capacity of 95, 84, and 65 mAh/g at 1, 2, and 5 C (1 C = 1.48 mA/cm²), respectively, in contrast to 89, 74, and 47 mAh/g for the pristine LMO. It indicates that hydrothermal treatment can eliminate the lattice defects and enhance the lithium diffusion kinetics inside the cycled and commercial particles.⁵⁴

Considering that spent LMO cells may have different SOHs, we also examined our regeneration approach using cells with a much higher degree of degradation. For example, a cell with 60% of capacity fading was obtained by cycling in a voltage range of 3.0–4.3 V for 500 cycles. Using the same regeneration protocol developed above, a LMO cathode with Li deficiency of up to 40% was fully recovered to the desired stoichiometry, which was supported by the compositions of cycled and regenerated LMO particles as shown in Table S4. In addition,

the undesired Li deficient phases were also converted back to the original spinel phase with the efficient relithiation process. Similar to the other samples, the electrochemical performance was also resumed to the same level of pristine LMO cathodes (Figure S6). The successful demonstration of direct regeneration of heavily degraded LMO cathode strongly suggests that our developed method can be applied to different cases of spent LMO cells.

Compared with traditional pyrometallurgical recycling and hydrometallurgical recycling, our direct regeneration method for closed-loop LMO recycling shows potential economic and environmental benefits, which were analyzed by the EverBatt model developed by Argonne National Laboratory⁵⁵ (see detailed methods in the Supporting Information).

In this model, by assuming 10 000 tons of spent LMO batteries annual processing capacity, the life-cycle analysis of the three different recycling methods was performed in terms of energy consumption, greenhouse gas (GHG) emission, operation cost, and overall profit. The flowchart for each recycling process is mentioned in Figures S9–11. In the pyrometallurgical process, the high-temperature smelting process not only consumes a large amount of energy but also generates exhaust gas. The following gas treatment process is necessary but expensive.^{56,57} In the hydrometallurgical process, most of the energy use comes from the upstream production of the strong acid/base/consumed for leaching and precipitation treatment. Figure 7a shows that a total energy

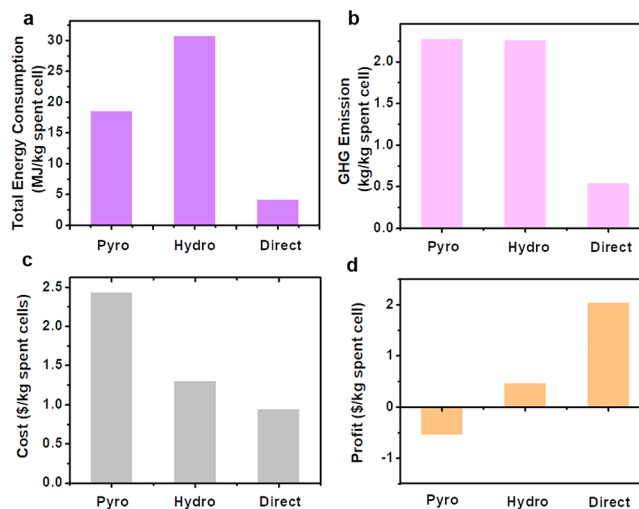


Figure 7. Life-cycle analysis based on the EverBatt model. (a) Total energy consumption and (b) GHG emissions per kg of recycled cells from pyrometallurgical, hydrometallurgical, and direct recycling, respectively. (c) Recycling cost and (d) profit per kg of spent LMO batteries obtained from pyrometallurgical, hydrometallurgical, and direct recycling, respectively.

consumption of 18.5 and 30.7 MJ per kg of spent cells is required in pyrometallurgical and hydrometallurgical processes, respectively. By comparison, the total energy consumption for direct recycling is only 4.1 MJ per kg of spent cells. Consistently, high GHG emission values are generated from burning fuels in both pyro- and hydrometallurgical processes (Figure 7b). In comparison, our direct regeneration process only accounts for around 20% of the GHG emission caused in the two traditional methods.

The cost and profit were also modeled, and the results are compared in Figure 7c and d. Compared with LCO and NCM cathodes, LMO has not been recycled on an industrial scale due to the low profit (or even economic loss).⁵⁸ The total cost of pyrometallurgical, hydrometallurgical, and direct recycling of LMO batteries was estimated to be \$2.43, \$1.3, and \$0.94 per kg of spent battery cells processed, respectively. It is worth to be mentioned that only the hydrometallurgical method collects manganese as manganese sulfate and manganese dioxide, while high-quality LMO cathode powder is obtained in the direct regeneration method. Since the current market value of LMO (\$7.00/kg) is much higher than that of Mn in product (\$1.43/kg), an economic benefit with a potential profit of \$2.03 per kg of spent cells can be obtained in the direct recycling process. In comparison, the expected profit in the pyrometallurgical method is calculated negatively. As the result of the significant reductions in total energy use, GHG emissions, and processing cost, as well as the potential increase of overall profit, the nondestructive, one-step aqueous direct regeneration method may be a preferable option for closed-loop LIB recycling. While the EverBatt model might have oversimplified the actual processing steps in the LIB recycling, we believe that the side-by-side comparison among the three recycling approaches can provide valuable guidance to select and improve the next-generation LIB recycling strategies.

CONCLUSION

In summary, we have successfully demonstrated complete regeneration of degraded LMO cathodes with different SOHs using a simple direct recycling approach. Particularly, the perfect reconstruction of desired stoichiometry and phase purity enabled by the one-step hydrothermal treatment in dilute Li-containing solutions provides the regenerated LMO particles with high capacity, long cycling stability, and high rate performance, on par with commercial pristine LMO materials. The understanding of the mechanism of the hydrothermal relithiation process provides a potential solution for sustainable and closed-loop remanufacturing of energy materials. The life-cycle analysis further suggests that our work represents a simple yet efficient approach to refunctionalize high-performance LMO cathodes, with distinct environmental and economic advantages over traditional pyrometallurgical and hydrometallurgical methods. Continuous improvement of the direct recycling method toward automated electrode separation and process intensification will pave the way for its practical application.

ASSOCIATED CONTENT

Supporting Information

The Supporting Information is available free of charge at <https://pubs.acs.org/doi/10.1021/acsami.0c15704>.

Experimental section, supplementary tables, and supplementary figures (electrochemical data, ICP data, Rietveld refinement of the XRD patterns, XPS fitting parameters, SEM images, TEM images, and EverBatt model) (PDF)

AUTHOR INFORMATION

Corresponding Author

Zheng Chen – Program of Materials and Science Engineering, Department of NanoEngineering, Program of Chemical Engineering, and Sustainable Power & Energy Center (SPEC),

University of California San Diego, La Jolla, California 92093, United States; orcid.org/0000-0002-9186-4298; Email: zhengchen@eng.ucsd.edu

Authors

Hongpeng Gao – Program of Materials and Science Engineering and Department of NanoEngineering, University of California San Diego, La Jolla, California 92093, United States

Qizhang Yan – Department of NanoEngineering, University of California San Diego, La Jolla, California 92093, United States

Panpan Xu – Department of NanoEngineering, University of California San Diego, La Jolla, California 92093, United States

Haodong Liu – Department of NanoEngineering, University of California San Diego, La Jolla, California 92093, United States

Mingqian Li – Department of NanoEngineering and Program of Chemical Engineering, University of California San Diego, La Jolla, California 92093, United States

Ping Liu – Program of Materials and Science Engineering, Department of NanoEngineering, and Sustainable Power & Energy Center (SPEC), University of California San Diego, La Jolla, California 92093, United States; orcid.org/0000-0002-1488-1668

Jian Luo – Program of Materials and Science Engineering, Department of NanoEngineering, and Sustainable Power & Energy Center (SPEC), University of California San Diego, La Jolla, California 92093, United States

Complete contact information is available at: <https://pubs.acs.org/10.1021/acsami.0c15704>

Notes

The authors declare the following competing financial interest(s): A Patent was filed for this work through the UCSD Office of Innovation and Commercialization. A Patent was filed for this work through the UCSD Office of Innovation and Commercialization.

ACKNOWLEDGMENTS

This work was supported by the US National Science Foundation via Award CBET-1805570, U.S. Department of Energy (DOE) via the ReCell Center, and the startup fund support from the Jacob School of Engineering at UC San Diego. Part of this work used the UCSD-MTI Battery Fabrication Facility and the UCSD-Arbin Battery Testing Facility. Neutron diffraction work was carried out at the Spallation Neutron Source (SNS), which is the U.S. DOE user facility at the Oak Ridge National Laboratory, sponsored by the Scientific User Facilities Division, Office of Basic Energy Sciences (BES). The electron microscopy work by Q.Y. and J.L. was supported as part of the Center for Synthetic Control Across Length-Scales for Advancing Rechargeables (SCALAR), an Energy Frontier Research Center funded by the US DOE, Office of Science, BES under Award No. DESC0019381.

REFERENCES

- (1) Placke, T.; Heckmann, A.; Schmuck, R.; Meister, P.; Beltrop, K.; Winter, M. Perspective on Performance, Cost, and Technical Challenges for Practical Dual-Ion Batteries. *Joule* **2018**, *2* (12), 2528–2550.
- (2) Etacheri, V.; Marom, R.; Elazari, R.; Salitra, G.; Aurbach, D. Challenges in the Development of Advanced Li-ion Batteries: a review. *Energy Environ. Sci.* **2011**, *4* (9), 3243–3262.
- (3) Blomgren, G. E. The Development and Future of Lithium Ion Batteries. *J. Electrochem. Soc.* **2017**, *164* (1), A5019–A5025.

- (4) Chen, M.; Ma, X.; Chen, B.; Arsenault, R.; Karlson, P.; Simon, N.; Wang, Y. Recycling End-of-Life Electric Vehicle Lithium-Ion Batteries. *Joule* **2019**, *3* (11), 2622–2646.
- (5) Zhang, Y.; Li, Y.; Tao, Y.; Ye, J.; Pan, A.; Li, X.; Liao, Q.; Wang, Z. Performance Assessment of Retired EV Battery Modules for Echelon Use. *Energy* **2020**, *193*, 116555.
- (6) Li, L.; Dunn, J. B.; Zhang, X. X.; Gaines, L.; Chen, R. J.; Wu, F.; Amine, K. Recovery of Metals from Spent Lithium-ion Batteries with Organic Acids as Leaching Reagents and Environmental Assessment. *J. Power Sources* **2013**, *233*, 180–189.
- (7) Zhang, X.; Li, L.; Fan, E.; Xue, Q.; Bian, Y.; Wu, F.; Chen, R. Toward Sustainable and Systematic Recycling of Spent Rechargeable Batteries. *Chem. Soc. Rev.* **2018**, *47* (19), 7239–7302.
- (8) Nie, H.; Xu, L.; Song, D.; Song, J.; Shi, X.; Wang, X.; Zhang, L.; Yuan, Z. LiCoO₂: Recycling from Spent Batteries and Regeneration with Solid State Synthesis. *Green Chem.* **2015**, *17* (2), 1276–1280.
- (9) Li, L.; Bian, Y.; Zhang, X.; Guan, Y.; Fan, E.; Wu, F.; Chen, R. Process for Recycling Mixed-cathode Materials from Spent Lithium-ion Batteries and Kinetics of Leaching. *Waste Manage.* **2018**, *71*, 362–371.
- (10) Yun, L.; Linh, D.; Shui, L.; Peng, X.; Garg, A.; LE, M. L. P.; Asghari, S.; Sandoval, J. Metallurgical and Mechanical Methods for Recycling of Lithium-ion Battery Pack for Electric vehicles. *Resources, Conservation and Recycling* **2018**, *136*, 198–208.
- (11) Yang, T.; Lu, Y.; Li, L.; Ge, D.; Yang, H.; Leng, W.; Zhou, H.; Han, X.; Schmidt, N.; Ellis, M.; Li, Z. An Effective Relithiation Process for Recycling Lithium-Ion Battery Cathode Materials. *Advanced Sustainable Systems* **2020**, *4* (1), 1900088.
- (12) Wang, S.; Wang, C.; Lai, F.; Yan, F.; Zhang, Z. Reduction-ammoniacal Leaching to Recycle Lithium, Cobalt, and Nickel from Spent Lithium-ion Batteries with a Hydrothermal Method: Effect of Reductants and Ammonium Salts. *Waste Manage.* **2020**, *102*, 122–130.
- (13) Wang, T.; Luo, H.; Bai, Y.; Li, J.; Belharouak, I.; Dai, S. Direct Recycling of Spent NCM Cathodes through Ionothermal Lithiation. *Adv. Energy Mater.* **2020**, *10* (30), 2001204.
- (14) Shi, Y.; Zhang, M.; Meng, Y. S.; Chen, Z. Ambient-Pressure Relithiation of Degraded Li_xNi_{0.5}Co_{0.2}Mn_{0.3}O₂ (0 < x < 1) via Eutectic Solutions for Direct Regeneration of Lithium-Ion Battery Cathodes. *Adv. Energy Mater.* **2019**, *9* (20), 1900454.
- (15) Shi, Y.; Chen, G.; Chen, Z. Effective regeneration of LiCoO₂ from Spent Lithium-ion Batteries: a Direct Approach towards High-performance Active Particles. *Green Chem.* **2018**, *20* (4), 851–862.
- (16) Shi, Y.; Chen, G.; Liu, F.; Yue, X.; Chen, Z. Resolving the Compositional and Structural Defects of Degraded LiNi_xCo_yMn_zO₂ Particles to Directly Regenerate High-Performance Lithium-Ion Battery Cathodes. *ACS Energy Letters* **2018**, *3* (7), 1683–1692.
- (17) Li, J.; Lu, Y.; Yang, T.; Ge, D.; Wood, D. L.; Li, Z. Water-Based Electrode Manufacturing and Direct Recycling of Lithium-Ion Battery Electrodes—A Green and Sustainable Manufacturing System. *iScience* **2020**, *23* (5), 101081.
- (18) Wang, H.; Whitacre, J. F. Direct Recycling of Aged LiMn₂O₄ Cathode Materials used in Aqueous Lithium-ion Batteries: Processes and Sensitivities. *Energy Technology* **2018**, *6* (12), 2429–2437.
- (19) Li, X.; Zhang, J.; Song, D.; Song, J.; Zhang, L. Direct Regeneration of Recycled Cathode Material Mixture from Scrapped LiFePO₄ Batteries. *J. Power Sources* **2017**, *345*, 78–84.
- (20) Bertuol, D. A.; Machado, C. M.; Silva, M. L.; Calgaro, C. O.; Dotto, G. L.; Tanabe, E. H. Recovery of Cobalt from Spent Lithium-ion batteries using Supercritical Carbon Dioxide Extraction. *Waste Manage.* **2016**, *51*, 245–251.
- (21) Wu, H. M.; Tu, J. P.; Yuan, Y. F.; Chen, X. T.; Xiang, J. Y.; Zhao, X. B.; Cao, G. S. One-step Synthesis LiMn₂O₄ Cathode by a Hydrothermal Method. *J. Power Sources* **2006**, *161* (2), 1260–1263.
- (22) Liu, Z.; Wang, W.-l.; Liu, X.; Wu, M.; Li, D.; Zeng, Z. Hydrothermal Synthesis of Nanostructured Spinel Lithium Manganese Oxide. *J. Solid State Chem.* **2004**, *177* (4), 1585–1591.
- (23) Kim, D. K.; Muralidharan, P.; Lee, H.-W.; Ruffo, R.; Yang, Y.; Chan, C. K.; Peng, H.; Huggins, R. A.; Cui, Y. Spinel LiMn₂O₄ Nanorods as Lithium Ion Battery Cathodes. *Nano Lett.* **2008**, *8* (11), 3948–3952.
- (24) Han, X.; Ouyang, M.; Lu, L.; Li, J. A Comparative Study of Commercial Lithium Ion Battery Cycle Life in Electric Vehicle: Capacity Loss Estimation. *J. Power Sources* **2014**, *268*, 658–669.
- (25) Zhan, C.; Lu, J.; Jeremy Kropf, A.; Wu, T.; Jansen, A. N.; Sun, Y.-K.; Qiu, X.; Amine, K. Mn(II) Deposition on Anodes and Its Effects on Capacity Fade in Spinel Lithium Manganate–Carbon Systems. *Nat. Commun.* **2013**, *4* (1), 2437.
- (26) Chung, K. Y.; Kim, K.-B. Investigation of Structural Fatigue in Spinel Electrodes Using In Situ Laser Probe Beam Deflection Technique. *J. Electrochem. Soc.* **2002**, *149* (1), A79–A85.
- (27) Chung, K. Y.; Kim, K.-B. Investigations into Capacity Fading as a result of a Jahn–Teller Distortion in 4V LiMn₂O₄ Thin Film Electrodes. *Electrochim. Acta* **2004**, *49* (20), 3327–3337.
- (28) An, K.; Skorpenske, H. D.; Stoica, A. D.; Ma, D.; Wang, X.-L.; Cakmak, E. First In Situ Lattice Strains Measurements under Load at VULCAN. *Metall. Mater. Trans. A* **2011**, *42* (1), 95–99.
- (29) An, K.; Wang, X.; Stoica, A. *Vulcan Data Reduction and Interactive Visualization Software*; ORNL Report; 2012; Vol. 621.
- (30) Toby, B. H. EXPGUI, a Graphical User Interface for GSAS. *J. Appl. Crystallogr.* **2001**, *34* (2), 210–213.
- (31) Larson, A.; Von Dreele, R. *General Structure Analysis System (GSAS)*; Technical Report LAUR 86-748; Los Alamos National Laboratory: Los Alamos, NM, 2004.
- (32) Appiah, W. A.; Park, J.; Byun, S.; Ryou, M.-H.; Lee, Y. M. A Mathematical Model for Cyclic Aging of Spinel LiMn₂O₄/Graphite Lithium-Ion Cells. *J. Electrochem. Soc.* **2016**, *163* (13), A2757–A2767.
- (33) Yunjian, L.; Xinhai, L.; HuaJun, G.; Zhixing, W.; Qiyang, H.; Wenjie, P.; Yong, Y. Electrochemical Performance and Capacity Fading Reason of LiMn₂O₄/graphite Batteries Stored at Room Temperature. *J. Power Sources* **2009**, *189* (1), 721–725.
- (34) Ryou, M.-H.; Han, G.-B.; Lee, Y. M.; Lee, J.-N.; Lee, D. J.; Yoon, Y. O.; Park, J.-K. Effect of Fluoroethylene Carbonate on High Temperature Capacity Retention of LiMn₂O₄/graphite Li-ion Cells. *Electrochim. Acta* **2010**, *55* (6), 2073–2077.
- (35) Hawley, W. B.; Parejiya, A.; Bai, Y.; Meyer, H. M.; Wood, D. L.; Li, J. Lithium and Transition Metal Dissolution due to Aqueous Processing in Lithium-ion Battery Cathode Active Materials. *J. Power Sources* **2020**, *466*, 228315.
- (36) Yuan, G.; Bai, J.; Doan, T. N. L.; Chen, P. Synthesis and Electrochemical Investigation of Nanosized LiMn₂O₄ as Cathode Material for Rechargeable Hybrid Aqueous Batteries. *Mater. Lett.* **2014**, *137*, 311–314.
- (37) Massarotti, V.; Capsoni, D.; Bini, M.; Azzoni, C. B.; Paleari, A. Stoichiometry of Li₂MnO₃ and LiMn₂O₄ Coexisting Phases: XRD and EPR Characterization. *J. Solid State Chem.* **1997**, *128* (1), 80–86.
- (38) Yang, X.; Tang, W.; Kanoh, H.; Ooi, K. Synthesis of Lithium Manganese Oxide in Different Lithium-containing Fluxes. *J. Mater. Chem.* **1999**, *9* (10), 2683–2690.
- (39) Kanamura, K.; Naito, H.; Yao, T.; Takehara, Z.-i. Structural Change of the LiMn₂O₄ Spinel Structure Induced by Extraction of Lithium. *J. Mater. Chem.* **1996**, *6* (1), 33–36.
- (40) Leifer, N.; Schipper, F.; Erickson, E. M.; Ghanty, C.; Talianker, M.; Grinblat, J.; Julien, C. M.; Markovsky, B.; Aurbach, D. Studies of Spinel-to-Layered Structural Transformations in LiMn₂O₄ Electrodes Charged to High Voltages. *J. Phys. Chem. C* **2017**, *121* (17), 9120–9130.
- (41) Kamarulzaman, N.; Yusoff, R.; Kamarudin, N.; Shaari, N. H.; Abdul Aziz, N. A.; Bustam, M. A.; Blagojevic, N.; Elcombe, M.; Blackford, M.; Avdeev, M.; Arof, A. K. Investigation of Cell Parameters, Microstructures and Electrochemical Behaviour of LiMn₂O₄ Normal and Nano Powders. *J. Power Sources* **2009**, *188* (1), 274–280.
- (42) Hao, X.; Lin, X.; Lu, W.; Bartlett, B. M. Oxygen Vacancies Lead to Loss of Domain Order, Particle Fracture, and Rapid Capacity Fade in Lithium Manganospinel (LiMn₂O₄) Batteries. *ACS Appl. Mater. Interfaces* **2014**, *6* (14), 10849–10857.

- (43) Putra, T. Y. S. P.; Yonemura, M.; Torii, S.; Ishigaki, T.; Kamiyama, T. Structure and Electrochemical Performance of the Spinel-LiMn₂O₄ Synthesized by Mechanical Alloying. *Solid State Ionics* **2014**, *262*, 83–87.
- (44) Sun, W.; Cao, F.; Liu, Y.; Zhao, X.; Liu, X.; Yuan, J. Nanoporous LiMn₂O₄ Nanosheets with Exposed {111} Facets as Cathodes for Highly Reversible Lithium-ion Batteries. *J. Mater. Chem.* **2012**, *22* (39), 20952–20957.
- (45) Tang, D.; Sun, Y.; Yang, Z.; Ben, L.; Gu, L.; Huang, X. Surface Structure Evolution of LiMn₂O₄ Cathode Material upon Charge/Discharge. *Chem. Mater.* **2014**, *26* (11), 3535–3543.
- (46) Kang, S.-H.; Goodenough, J. B.; Rabenberg, L. K. Nanocrystalline Lithium Manganese Oxide Spinel Cathode for Rechargeable Lithium Batteries. *Electrochem. Solid-State Lett.* **2001**, *4* (5), A49–A51.
- (47) Lee, S.; Oshima, Y.; Hosono, E.; Zhou, H.; Kim, K.; Chang, H. M.; Kanno, R.; Takayanagi, K. In Situ TEM Observation of Local Phase Transformation in a Rechargeable LiMn₂O₄ Nanowire Battery. *J. Phys. Chem. C* **2013**, *117* (46), 24236–24241.
- (48) He, H.; Cong, H.; Sun, Y.; Zan, L.; Zhang, Y. Spinel-layered Integrate Structured Nanorods with Both High Capacity and Superior High-rate Capability as Cathode Material for Lithium-ion batteries. *Nano Res.* **2017**, *10* (2), 556–569.
- (49) Nesbitt, H. W.; Banerjee, D. Interpretation of XPS Mn(2p) Spectra of Mn Oxyhydroxides and Constraints on the Mechanism of MnO₂ Precipitation. *Am. Mineral.* **1998**, *83* (3–4), 305–315.
- (50) Chen, Y.; Tian, Y.; Qiu, Y.; Liu, Z.; He, H.; Li, B.; Cao, H. Synthesis and Superior Cathode Performance of Sandwiched LiMn₂O₄@rGO nanocomposites for lithium-ion batteries. *Materials Today Advances* **2019**, *1*, 100001.
- (51) Hosono, E.; Kudo, T.; Honma, I.; Matsuda, H.; Zhou, H. Synthesis of Single Crystalline Spinel LiMn₂O₄ Nanowires for a Lithium Ion Battery with High Power Density. *Nano Lett.* **2009**, *9* (3), 1045–1051.
- (52) Chen, K.-S.; Xu, R.; Luu, N. S.; Secor, E. B.; Hamamoto, K.; Li, Q.; Kim, S.; Sangwan, V. K.; Balla, I.; Guiney, L. M.; Seo, J.-W. T.; Yu, X.; Liu, W.; Wu, J.; Wolverton, C.; Druvid, V. P.; Barnett, S. A.; Lu, J.; Amine, K.; Hersam, M. C. Comprehensive Enhancement of Nanostructured Lithium-Ion Battery Cathode Materials via Conformal Graphene Dispersion. *Nano Lett.* **2017**, *17* (4), 2539–2546.
- (53) Yu, L.; Qiu, X.; Xi, J.; Zhu, W.; Chen, L. Enhanced High-potential and Elevated-Temperature Cycling Stability of LiMn₂O₄ Cathode by TiO₂ Modification for Li-ion Battery. *Electrochim. Acta* **2006**, *51* (28), 6406–6411.
- (54) Cabana, J.; Valdés-Solís, T.; Palacín, M. R.; Oró-Solé, J.; Fuertes, A.; Marbán, G.; Fuertes, A. B. Enhanced High Rate Performance of LiMn₂O₄ Spinel Nanoparticles Synthesized by a Hard-template Route. *J. Power Sources* **2007**, *166* (2), 492–498.
- (55) Dai, Q.; Spangenberg, J.; Ahmed, S.; Gaines, L.; Kelly, J. C.; Wang, M. *EverBatt: A Closed-Loop Battery Recycling Cost and Environmental Impacts Model*; Argonne National Laboratory: Argonne, IL, 2019.
- (56) Ciez, R. E.; Whitacre, J. F. Examining Different Recycling Processes for Lithium-ion batteries. *Nature Sustainability* **2019**, *2* (2), 148–156.
- (57) Ellingsen, L. A.-W.; Hung, C. R.; Strømman, A. H. Identifying Key Assumptions and Differences in Life Cycle Assessment Studies of Lithium-ion Traction Batteries with Focus on Greenhouse Gas Emissions. *Transportation Research Part D: Transport and Environment* **2017**, *55*, 82–90.
- (58) Winslow, K. M.; Laux, S. J.; Townsend, T. G. A Review on The Growing Concern and Potential Management Strategies of Waste Lithium-ion Batteries. *Resources, Conservation and Recycling* **2018**, *129*, 263–277.